Ultrasensitive nonlinear vibrational spectroscopy of complex molecular systems

Selig, O.

[Link to publication](#)

CHAPTER 5

ULTRASENSITIVE ULTRAFAST VIBRATIONAL SPECTROSCOPY EMPLOYING THE NEAR FIELD OF GOLD NANOANTENNAS[a]

We introduce a novel method to perform nonlinear vibrational spectroscopy on nanoscale volumes. Our technique uses the intense near field of infrared nanoantennas to amplify the nonlinear vibrational signals of molecules located in the vicinity of the antenna surface. We demonstrate the capabilities of the method by performing infrared pump-probe spectroscopy and two-dimensional infrared (2DIR) spectroscopy on 5 nm layers of polymethylmetacrylate (PMMA). In these experiments we observe enhancement factors of the nonlinear signals of more than 4 orders of magnitude. We discuss the mechanism underlying the amplification process as well as strategies for further increasing the sensitivity of the technique.

5.1 Introduction

Vibrational spectroscopy is a powerful, label-free technique that provides detailed information about molecular structures. The method uses vibrational marker modes to identify the chemical groups present inside a molecule as well as to probe their chemical nanoenvironments. In recent years vibrational spectroscopy has experienced a revival with the advent of novel, *nonlinear* vibrational spectroscopies, in particular infrared pump-probe spectroscopy and two-dimensional infrared (2DIR) spectroscopy.[138–142] In these techniques the sample is interrogated by a number of time-delayed femtosecond infrared pulses, allowing one to study not only the structures of molecules but also their dynamics.[25, 143–145] While these two nonlinear methods are mostly applied to macroscopic samples, they could in principle provide valuable information about nanoscale systems consisting of molecular monolayers, such as the active areas of biosensors, supported lipid bilayers, and responsive surfaces.[146, 147] Unfortunately, because of the low absorption cross-section of molecular vibrations, the only molecular monolayers that are amenable to study using these techniques are those composed of extremely strong infrared absorbers: in particular, to date such measurements have only been reported for metal-carbonyl compounds.[148, 149] Obviously, a method allowing for the application of these nonlinear spectroscopies to other, less absorptive, molecular vibrations at the (sub)monolayer level would be highly beneficial.

An attractive option for amplifying the interaction of molecular vibrations with infrared radiation is the use of optical nanoantennas. These metallic nanostructures have recently attracted considerable interest due to their ability to funnel light to subwavelength volumes and thereby strongly enhance the local electromagnetic field.[49, 150] Particularly strong field enhancements can be achieved with the help of resonant nanostructures, such as rod-shaped nanoantennas, which exhibit a dipolar resonance that can be tuned all the way from the visible spectral region to the far infrared, simply by varying the length of the nanoantenna. In the past it has been demonstrated that infrared-resonant nanoantennas can strongly amplify the linear vibrational spectroscopic signals of molecules located in their near fields.[37, 151–154] In addition nonlinear frequency-mixing processes such as second-harmonic generation,[155] third-harmonic generation[156] and four-wave mixing[157, 158] have been demonstrated to occur in the near fields of nanoantennas. An application that has not been explored to date is the use of infrared nanoantennas as a means to perform highly efficient nonlinear spectroscopy. Recently it was demonstrated that nonlinear vibrational signals (2DIR) can be enhanced using colloidal gold nanoparticles,[159] but the possibilities provided by nanoantenna structures designed to be resonant with a specific vibrational mode have not yet been exploited.

Here we report on a proof-of-principle experiment in which we use the enhanced near field of nanoantenna arrays to perform femtosecond vibrational pump-probe spectroscopy on the carbonyl vibration of ultrathin layers of polymethylmetacrylate (PMMA) deposited on top of the arrays. The enhanced near field of the nanoantennas decays rapidly with distance, and, consequently, we only probe those regions of the PMMA film located directly on top of the nanoantennas. We demonstrate that with this method the nonlinear spectroscopic signals are amplified by more than 4 orders
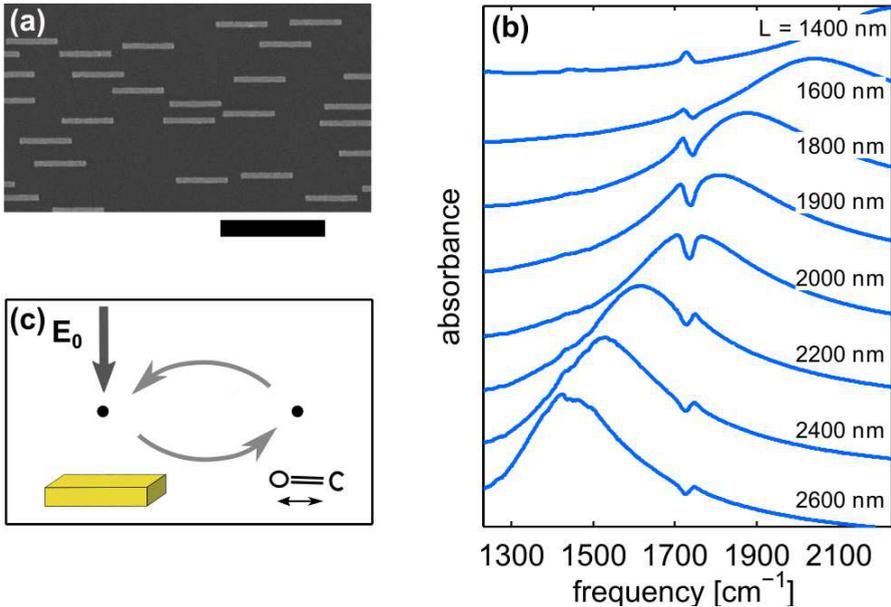
FIGURE 5.1. a) Scanning electron microscope (SEM) image of one of the antenna arrays. The scale bar corresponds to a distance of 4 μm. (b) Infrared absorbance spectra (light polarized along the long antenna axis) of randomized nanoantenna arrays coated with a 14 nm layer of PMMA. The spectra are offset vertically for clarity. (c) Schematic representation of the coupled-dipole model described in the text. Both the nanoantenna and the PMMA patch on top are represented as point dipoles.

of magnitude.

5.2 LINEAR INFREARED SPECTROSCOPY

In our experiments we use gold nanoantenna arrays that are fabricated on CaF_2 substrates using standard e-beam lithography (for a detailed description see Section 3.5). The antennas are arranged in 800 μm × 800 μm randomized arrays at a density of 0.17 μm^{-2} (Fig. 5.1(a)). The random antenna arrangement serves to average out the effects of coupling between the individual antennas.[151] The antennas are 200 nm wide, 100 nm high, and their length varies between 1400 and 2600 nm. Antennas of these lengths interact strongly with midinfrared light that is polarized along the long antenna axis. This is illustrated in Fig. 5.1(b) where we show the IR transmission spectra of a number of antenna arrays that are covered with a 14 nm layer of PMMA. These spectra were recorded with a Bruker Vertex 80v FTIR spectrometer coupled to a Hyperion 3000 IR microscope. The longitudinal plasmon resonance has a width of 300–500 cm^{-1} and the resonance shifts to the red with increasing antenna length.[152] In addition a small modulation on top of the antenna spectrum is observed around

1730 cm^{-1}, which is due to the interaction with the PMMA carbonyl vibration. The spectra in Fig. 5.1(b) illustrate that the antennas do not merely amplify the *absorption* by the PMMA: in that case one would observe positive absorptive peaks on top of the antenna spectra (i.e., an increased absorption). Instead the enhancement mechanism leads to complex vibrational line shapes that depend on the detuning between the vibrational transition and the antenna resonance.[152] In the following we use a simple, coupled-dipole model[160, 161] to explain the observed line shapes and their intensities (Fig. 5.1(c)). An extended discussion of this model will be presented in Chapter 6. In order to keep the notation simple we use a scalar description. We treat the antenna and the PMMA patch on top of it as two dipolar point scatterers with respective complex polarizabilities $\alpha_{\text{ant}}(\omega)$ and $\alpha_{\text{vib}}(\omega)$ and locations r_{ant} and r_{vib}. We note that both polarizabilities are frequency dependent: $\alpha_{\text{vib}}(\omega)$ due to the vibrational resonance of the CO vibration of PMMA, and $\alpha_{\text{ant}}(\omega)$ due to the plasmonic antenna resonance (tunable by varying the antenna length). The incident electric field $E_0(\omega)$ polarizes the antenna, which leads to an enhanced near field that induces a vibrational dipole given by

$$p_{\text{vib}}(\omega) = \alpha_{\text{vib}}(\omega)G(r_{\text{vib}}, r_{\text{ant}})\alpha_{\text{ant}}(\omega)E_0(\omega) \tag{5.1}$$

where $G(r_{\text{vib}}, r_{\text{ant}})$ is the Green function for a radiating dipole located at position r_{ant}. In this expression we have neglected the contribution of the incident field itself to the vibrational polarization as its effect is much smaller than that of the local field. The induced vibrational dipole acts back and induces a change in the antenna polarization

$$\Delta p_{\text{ant}}(\omega) = \alpha_{\text{ant}}(\omega)G(r_{\text{ant}}, r_{\text{vib}})p_{\text{vib}}(\omega) \tag{5.2}$$

Combining these expressions and using the fact that the extinction cross section of the antenna $\sigma_{\text{ant}}(\omega)$ is given by the ratio of the work done on the antenna by the *incident* field $\frac{1}{2}\omega\text{Im}[p_{\text{ant}}(\omega)E_0^*(\omega)]$ to the incident intensity we arrive at the following expression for the modification of the antenna cross section due to the presence of the PMMA

$$\Delta\sigma_{\text{ant}}(\omega) = \frac{2\pi}{\lambda\varepsilon_0}\text{Im}\left\{[\alpha_{\text{ant}}(\omega)G]^2 \alpha_{\text{vib}}(\omega)\right\} \tag{5.3}$$

In this equation λ is the free-space wavelength and ε_0 is the permittivity of free space. We have used the reciprocity relation to equate the two appearing Green functions and simply denoted them by G. Despite the approximations made in the above treatment this equation provides an excellent description of the antenna-enhanced vibrational line shapes, as we have confirmed through finite-difference time domain simulations (see Chapter 6). Equation 5.3 shows that the nanoantenna amplifies the original vibrational spectrum by the complex-valued factor $(\alpha_{\text{ant}}(\omega)G)^2$, which represents the square of the field enhancement. Because of the complex nature of the amplification factor the (enhanced) vibrational signal $\Delta\sigma_{\text{ant}}(\omega)$ typically contains both an absorptive $\text{Im}[\alpha_{\text{vib}}(\omega)]$ and a dispersive $\text{Re}[\alpha_{\text{vib}}(\omega)]$ component as can be seen in Fig. 5.1(b). It is straightforward to see that there are three circumstances under which purely absorptive line shapes are observed: if the antenna is driven on resonance, far below resonance, or far above resonance. In the first case there is a
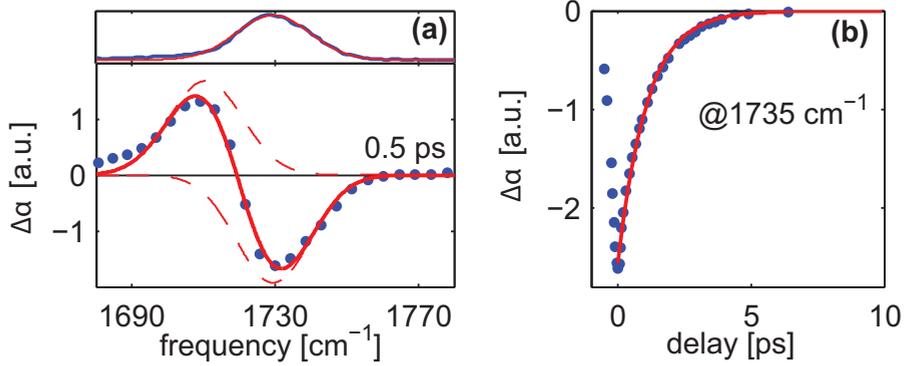
FIGURE 5.2. (a) Top: Linear infrared spectrum (blue line) of the carbonyl vibration of a 150 nm film of PMMA on a CaF$_2$ substrate. The red line represents a Gaussian fit. Bottom: Transient spectrum of the same sample (isotropic signal). The solid red line is a fit to a linear combination of two Gaussian bands (dashed lines) whose widths are taken from the linear spectrum. b) Delay scan of the transient signal at a frequency of 1735 cm^{-1}. The red line is a monoexponential fit.

$\pi/2$ phase lag between the incident electric field and the antenna polarization: this leads to a negative value ($(e^{i\pi/2})^2 = -1$) of the amplification factor $(\alpha_{ant}(\omega)G)^2$, so that the vibrational signal is observed as an absorption *dip* on top of the antenna resonance. Driving the antenna far below resonance or far above resonance results in phase shifts of 0 and π, respectively, so that in these two circumstances absorptive *peaks* ($(e^{i0})^2 = -1$ and $(e^{i\pi})^2 = -1$) are observed.

5.3 PUMP-PROBE SPECTROSCOPY

We investigate the nonlinear optical properties of the PMMA-covered arrays using femtosecond IR pump-probe spectroscopy (see Chapter 3 for a detailed description of the experimental setup). In these measurements we use a femtosecond ($\sim$100 fs, 150 nJ) infrared pulse centered at 1700 cm^{-1} to excite a significant fraction of the carbonyl vibrations in the PMMA layer. The pump-induced absorption changes ($\Delta\alpha = -\ln T/T_0$) are monitored by a delayed probe pulse. In order to perform polarization-resolved measurements the probe polarization is set at an angle of 45 deg with respect to the pump polarization. Using polarizers behind the sample we then select the probe component that is polarized either parallel or perpendicular to the pump polarization. Scattered pump light is suppressed by rapidly modulating the pump-probe delay by half an optical period.[162]

As a reference measurement the pump-probe spectrum of a thick layer of PMMA ($\sim$150 nm) deposited on a CaF$_2$ substrate is shown in Fig. 5.2. We observe the characteristic transient spectrum of an anharmonic vibration. At the fundamental frequency (1730 cm^{-1}) there is a decreased absorption due to the depletion of the

ground state and stimulated emission from the vibrationally excited state. At lower frequencies ($\sim$1710 cm^{-1}) an induced absorption is observed due to absorption by the excited state. A fit of the transient spectrum to a linear combination of two Gaussian bands reveals an anharmonicity of 19 cm^{-1}. The ratio of the 0-1 and 1-2 cross sections is 1.8, which is very close to the value of 2 expected for a purely harmonic vibration. Figure 5.2(b) shows a delay scan for a frequency corresponding to the peak of the bleach ($\sim$1735 cm^{-1}). We observe a monoexponential decay with a time constant of 1.1 ps which we attribute to the vibrational relaxation of the carbonyl vibration.

Having characterized the transient vibrational response of PMMA itself we move on to study the effect of coupling with the nanoantennas. For this purpose we work with a 5 nm film of PMMA (see Section 5.6.2 for the determination of the thickness), which gives no appreciable pump-probe signal in the absence of antennas: the smallest signal we could detect ($\Delta\alpha = 2 \times 10^{-5}$) was for a 10 nm thick film, which is shown in Fig. 5.3(a). Next we consider the situation of a 5 nm film deposited on an array of nanoantennas ($L = 2000$ nm) that are tuned to resonance with the carbonyl vibration. Figure 5.3(b) shows the pump-probe signal for a measurement in which the pump pulse is polarized parallel to the long axis of the antennas and the probe pulse is polarized along the short antenna axis. Remarkably even though the (perpendicularly polarized) probe is not resonant with the antennas, we nevertheless observe an increase in the nonlinear signal by a factor of 100. Next we polarize the probe along the long axis of the nanoantennas (Fig. 5.3(c)). We observe a further increase of the nonlinear signal to a value as high as $\Delta\alpha = 0.055$. In addition we see that the sign of the nonlinear signal is inverted compared to the reference signals in Figs. 5.2(a) and 5.3(a). This inversion can be understood from the linear spectrum of the 2000 nm antennas in Fig. 5.1(b). As was explained above, in this case the coupling to the nanoantennas is such that the presence of the carbonyl vibration leads to a decrease of the absorption. As a consequence the depletion of the ground state of this vibration by a pump pulse leads to an increased absorption while the coupling of the antennas with the newly accessible $1 \rightarrow 2$ transition leads to a decreased absorption. We note that when the antennas are probed along their short axis we also observe an enhancement of the nonlinear signal (Fig. 5.3(b)). In this case the nonlinear signal has the regular sign: a decreased absorption at the fundamental frequency and an increased absorption at the excited-state frequency. This nonlinear signal originates from the coupling of the excited vibrations (and the depleted ground state) with the transverse resonance of the nanoantennas, which lies at much higher frequencies in the visible spectral region.[163] The normal sign follows from the fact that the vibrations drive this transverse antenna mode far below its resonance frequency, which, according to Eqn. (5.3), leads to a positive (and real-valued) amplification factor in the linear spectrum and therefore also in the nonlinear spectrum.

It should be noted that the nonlinear signal in Fig. 5.3(c) originates from only a small fraction of the CO vibrations on the substrate (i.e. those vibrations located close to the antenna surface). The nonlinear signal enhancement is, therefore, much larger than the ratio of the absorption changes in Figs. 5.3(a) and (c). The question arises of how large the enhancement actually is. The nonlinear signal is described by an equation identical to Eqn. (5.3) except for the replacement of $\alpha_{\text{vib}}(\omega)$ by the pump-induced change $\Delta\alpha_{\text{vib}}(\omega)$, which is proportional to the number of excited
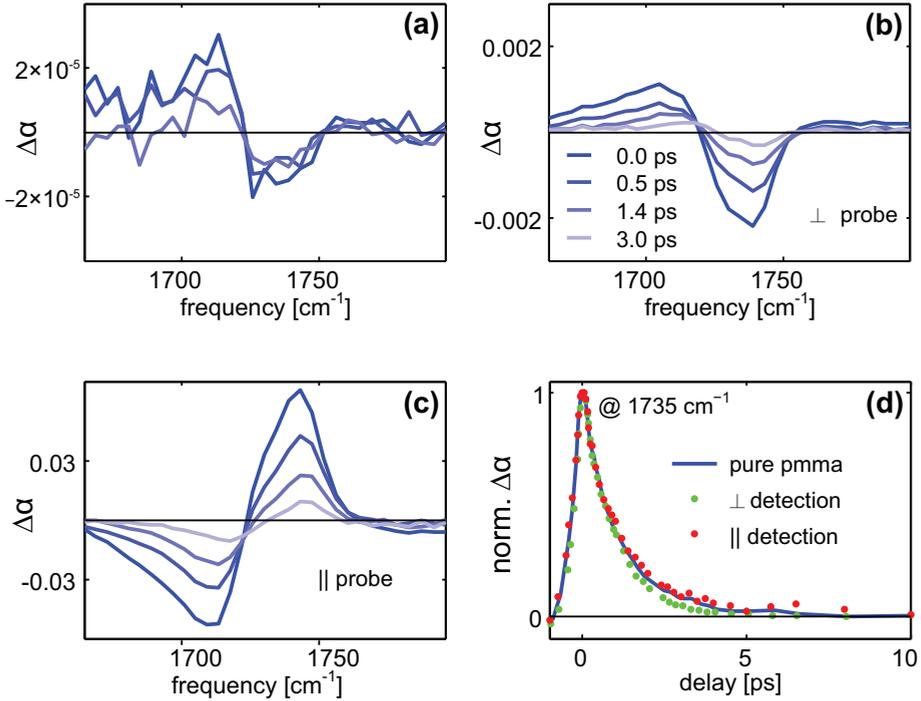
FIGURE 5.3. a) Transient spectrum of a 10 nm layer of PMMA on CaF_2 (isotropic signal). b) Transient signal for a 5 nm PMMA film deposited on top of nanoantennas. The pump polarization is along the long axis of the antenna while the probe polarization is along the short axis. c) Transient signal for the same sample as in (b) with the pump and probe polarizations set parallel to the long axis of the antennas. (d) Normalized delay traces at 1735 cm^{-1} for the reference measurement on a 150 nm layer of PMMA (blue line) and for a 5 nm layer of PMMA on a nanoantenna array ($L = 2000$ nm) with a perpendicular probe (red dots) and a parallel probe (green dots).

vibrations and therefore to the local field *intensity*. Since $\alpha_{ant}(\omega)G$ represents the field enhancement, the nonlinear signal is proportional to the fourth power of the field enhancement. Using this result in combination with finite-difference time domain simulations, we find that more than 90% of the nonlinear signal originates from CO vibrations that are within 40 nm of the antenna surface. This means that the nonlinear signal in Fig. 5.3(c) originates from 10% of the CO vibrations covering the antenna array (the nanoantennas cover 7% of the surface), from which a net enhancement factor of 6×10^4 for the nonlinear spectrum in Fig. 5.3(c) can be determined (see Section 5.6.1 for details).

Next we turn to the time dependence of the enhanced vibrational signal. An important point is whether the temporal decay of the signal tracks the excited state population of the carbonyl vibration or whether it is affected nontrivially by the coupling with the nanoantenna. To investigate this issue we compare the delay traces

of the enhanced signals (i.e. for parallel and perpendicular probing) with the delay trace of the unenhanced reference measurement (Fig. 5.3(d)). The strong resemblance of the three signals demonstrates that the enhanced signals indeed accurately reflect the intrinsic vibrational dynamics of the molecular system (and therefore provide information about the molecular system itself).

5.4 TWO-DIMENSIONAL INFRARED SPECTROSCOPY

The high signal strength and excellent signal-to-noise ratio of the antenna-enhanced pump-probe spectra (Fig. 5.3(c)) allows us to move beyond one-color pump-probe spectroscopy and explore the capabilities of antenna enhancement in 2DIR spectroscopy. We employ a pumping technique in which a Mach-Zehnder interferometer is used to generate a pair of collinear pump pulses.[78] Transient spectra are recorded as a function of the delay between the two pump pulses, and Fourier transformation of this time variable yields the pump-frequency axis in the two-dimensional spectrum (see Section 3.3 for additional details). Figure 5.4 shows examples of 2DIR spectra for two different antenna fields ($L = 1900$ nm and $L = 2200$ nm) coated with 5 nm of PMMA. The pronounced diagonal elongation in these spectra indicates that the carbonyl band of PMMA is in fact composed of an inhomogeneous distribution of CO oscillators that can be excited independently of each other: the band shows strong inhomogeneous broadening. In passing we note that a homogeneously broadened band would show a nearly vertical central line. A measure for the degree of inhomogeneous broadening is provided by the tilt of the central line, which is drawn in the 2D spectra. The two spectra in Fig. 5.4 exhibit different two-dimensional line shapes reflecting the difference in the corresponding linear line shapes. Nevertheless, the central line slope is identical for both spectra (1.2 ± 0.1) indicating that this parameter can be extracted quite robustly from the antenna-enhanced 2D spectra. In the future it will be interesting to perform these measurements as a function of the pump-probe delay, which will provide information about the time scale on which spectral fluctuations occur.

5.5 OUTLOOK

An obvious question that arises after these proof-of-principle experiments is how far we are removed from performing nonlinear vibrational spectroscopy on molecular monolayers, such as supported lipid membranes. From the density and molecular weight of PMMA we estimate that a 5 nm layer of PMMA contains ~35 CO groups/nm^2. For a lipid bilayer this number is ~6 CO groups/nm^2 as can be deduced from the typical surface area of 0.7 nm^2 per lipid molecule.[164] This comparison shows that we are already within an order of magnitude of the required sensitivity. Given that the nonlinear signal in our experiments scales with the fourth power of the field enhancement, an obvious way to increase the sensitivity would be to use nanostructures which provide higher field enhancements. Examples of structures that could provide exceptionally high field enhancements are optimally coupled arrays of nanoantennas,[163] fractal-shaped antennas[153] and perfect-absorber
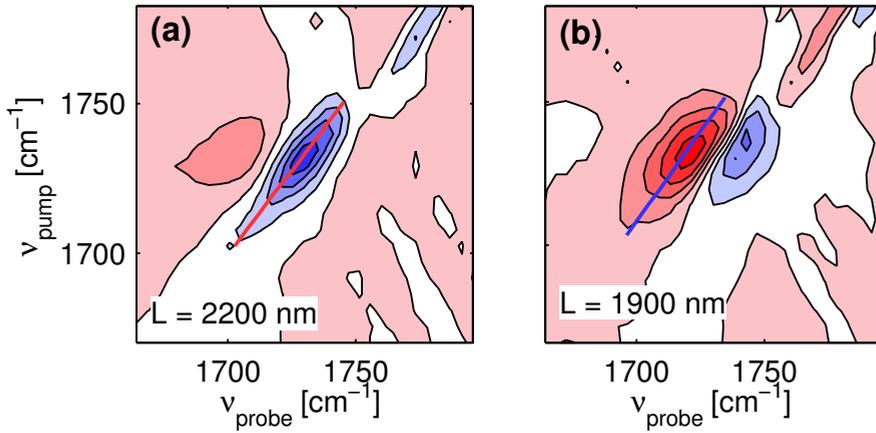
FIGURE 5.4. 2DIR spectra of 5 nm PMMA on nanoantennas of (a) 2200 nm and (b) 1900 nm. The thin solid lines represent equidistantly spaced contours. Positive absorption changes are shown in red and negative absorption changes in blue. The spectra correspond to a pump-probe delay of 0.5 ps. The thick solid lines represent the central lines and are calculated by fitting the locations of the local maxima of the 2D spectra to a straight line.

metamaterials.[165] In conclusion, we have demonstrated that metallic nanoantennas can be used to amplify nonlinear vibrational signals by more than 4 orders of magnitude. This new technique will allow the study of molecular structures and dynamics of nanoscopic volumes including molecular monolayers.

5.6 APPENDIX

5.6.1 CALCULATION OF THE ENHANCEMENT FACTOR FOR THE NONLINEAR SIGNAL

In this section we outline the procedure used to determine the amplification factor of the nonlinear spectrum in Figure 5.3(c). To compute this amplification factor we need to estimate how far the influence of a nanoantenna extends beyond its surface. This characteristic distance depends on the field enhancement profile around the nanoantenna, which was calculated using finite-difference time domain simulations (for details see Chapter 6) and is displayed in Figure 5.5(a). The figure shows the absolute value of the field enhancement in a plane 5 nm above the substrate. As was explained previously the nonlinear signal is proportional to the fourth power of the field enhancement. Using these results we can determine how close a CO vibration should be to the antenna surface in order to still make a reasonably-sized contribution to the nonlinear signal. To this end we compute the integrated nonlinear signal that would originate from a strip-like region surrounding the nanoantenna (see inset of Figure 5.5(b)). We have plotted this quantity as a function of the strip width ΔL in Figure 5.5(b). The plot shows that more than 90% of the nonlinear signal originates from CO vibrations that are within 40 nm of the antenna surface (the value of 90% is a lower limit because the contribution of the CO vibrations located on top of the nanoantenna has not been taken into account). Consequently for a single nanoantenna of 2000 nm by 200 nm the nonlinear signal originates from a patch of PMMA with a surface area that is 45% larger than the footprint of the nanoantenna. We therefore conclude that the nonlinear signal in Figure 5.3(c) originates from 10% of the CO vibrations covering the whole substrate (the nanoantennas cover 7% of the surface).

The ratio of the absorption changes in Figure 5.3(a) and (c) is 3×10^3. We take into account that the reference spectrum in Figure 5.3(a) corresponds to a 10 nm layer of PMMA while the spectrum in Figure 5.3(c) is for a 5 nm layer, and that the amplified nonlinear signal originates from 10% of the molecules on the substrate. This gives the net amplification factor of 6×10^4 quoted in the main text.

5.6.2 THICKNESS DETERMINATION OF THE PMMA LAYERS

The PMMA films used in the experiments were produced by spin coating from solution (mr-I PMMA, micro resist technology GmbH). A spinning speed of 4000 rpm was used, and the layer thickness was varied by diluting the stock solution in anisole. The layer thickness was determined through a combination of ellipsometry, profilometry and IR transmission spectroscopy. Due to the relative softness and roughness of CaF_2 profilometry could only provide accurate data for a relatively thick layer (25 nm) of PMMA on CaF_2. The thickness of the thinner layers was determined from the IR absorption of the carbonyl band. As a reference we also determined the layer thickness for other substrates (silicon and glass), using ellipsometry and profilometry. Figure 5.6 displays the full calibration series.
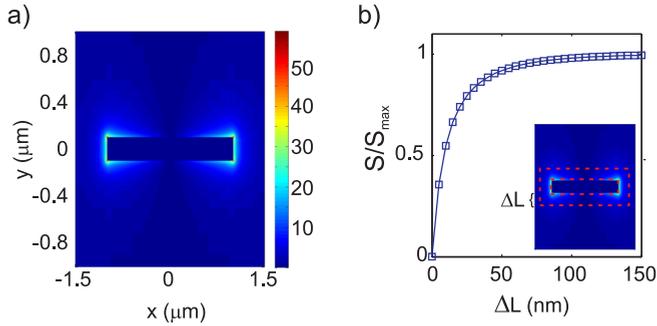
FIGURE 5.5. a) Field enhancement for a nanoantenna of 2000 nm on a CaF$_2$ substrate. The calculation pertains to a height of 5 nm above the substrate. b) Total nonlinear signal originating from the region between the two red dashed rectangles in the inset. This quantity was obtained by integrating the fourth power of the field enhancement over this region. The inner rectangle has the same dimensions as the nanoantenna; the outer rectangle extends beyond the nanoantenna surface by a distance ΔL. The integrated signal is normalized to its limiting value for large values of ΔL.
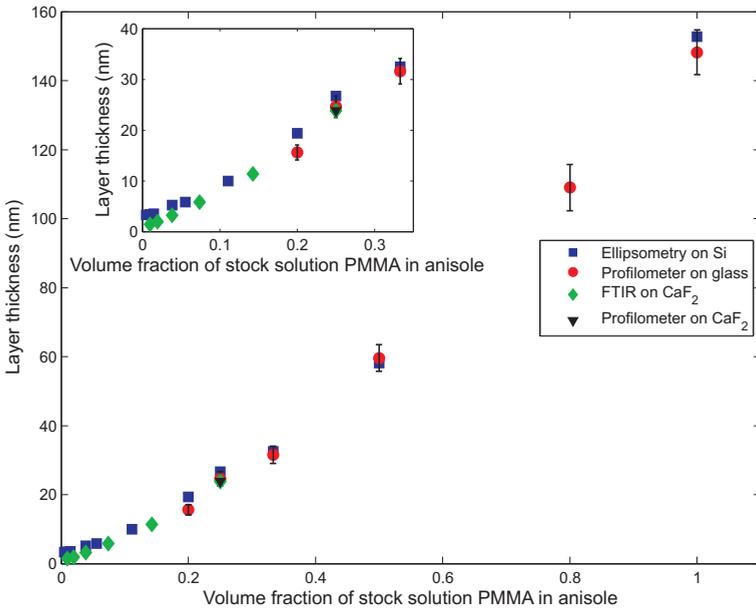

FIGURE 5.6. Thickness of the PMMA layers determined using different methods.